Article

Stability Analysis of Retaining Walls with Geocell-Reinforced Road Milling Materials

Bingbing Zhang, Fei Song * and Weiguang Li

School of Highway Engineering, Chang'an University, Xi'an 710064, China
* Correspondence: songf1980@163.com

Abstract: A series of triaxial compression tests with different confining pressures were conducted for gravels, road surface milling materials, and surface–base milling mixtures to investigate the stress–strain relationships of these three kinds of materials. On the basis of the analysis of the test results, the strength and the deformation of the geocell-reinforced surface milling materials and the geocell-encased surface–base milling mixtures were predicted and compared with those of the gravels via the constitutive model of geocell–soil composites. The effects of the geocell pocket size, tensile stiffness, and the peak internal frictional angle on the stress–strain responses of the geocell-reinforced surface–base milling mixtures were examined. Moreover, by employing the finite element strength reduction technique, stability analysis was conducted on the geocell-reinforced retaining wall with the surface–base milling mixtures to investigate the factor of safety and the failure mechanism of the structure. The study results indicated that the surface milling materials exhibited strain hardening, while the gravels and the surface–base milling mixtures exhibited strain softening. The surface milling materials displayed evident shear contraction characteristics, whereas the gravels and surface–base milling mixtures first displayed shear contraction and later dilatancy features. In addition, the strength of the geocell-reinforced surface milling materials is smaller than that of the gravels, but the strength of the geocell-encased surface–base milling mixtures is larger than that of the gravels. Thus, the geocell-reinforced surface–base milling mixtures can be used to replace the gravels in engineering practices. Additionally, the size of the sliding wedge and the factor of safety of the retaining walls increase significantly with reductions in the geocell pocket size.

Keywords: triaxial compression tests; road milling materials; geocell; strength reduction technique; stability analysis

1. Introduction

In recent years, due to the increasing demands of the transportation infrastructural developments, highway reconstruction and expansion, renovation, and upgrading have become key projects (Hessam et al., 2019 [1]; Li et al., 2014 [2]). In the process of road renovation, a large amount of recycled road milling materials will be produced. These abandoned road milling materials generally show poor mechanical and engineering properties and are difficult to recycle and reuse. As a result, how to re-apply abandoned asphalt milling materials in engineering practices has become an urgent problem (Li et al., 2015 [3]; Klauer et al., 2020 [4]; Masi et al., 2015 [5]; Lu et al., 2015 [6]).

The mechanical properties of the abandoned road milling materials have been experimentally investigated by some researchers. Rafiqul et al. (2016) [7] investigated the effects of cement content and asphalt milling materials on the mechanical characteristics of a cold recycled milling material mixture, including splitting strength, compressive strength, and compressive springback modulus. By performing splitting fatigue experiments on core samples taken from cold-reclaimed pavements, Okan et al. (2016) [8] examined the fatigue properties of cold-reclaimed milling materials at various stress ratios and thicknesses. Wu et al. (2021) [9] studied the influences of the cement dosage, the composition

of milling materials, the temperature, and the health age on the unconfined compressive strength, the flexural strength, and the compressive resilience modulus of the mixture through laboratory tests. Yu et al. (2022) [10] determined the performance parameters such as the optimal asphalt dosage and the Marshall stability by conducting Marshall tests on the asphalt milling materials with different mix ratios. At present, the engineering mechanical properties of the asphalt milling materials are improved mainly by adding different cement contents. The reasonable cement content of asphalt milling materials can be obtained via analyzing the improved mechanical properties by cement mixing, such as splitting strength, fatigue characteristics, and compressive resilience modulus of asphalt milling materials. However, because the technology of asphalt milling materials improved by cement mixing lead to rigid reinforcement, its service life durability is poor when the process is subjected to cyclic loads. Thus, it has not been widely popularized and applied.

A geocell is a type of three-dimensional honeycombed cellular geosynthetic made from polymeric sheets (e.g., high density polyethylene, HDPE) interconnected by ultrasonically welded seams. It has significant advantages over planar reinforcement materials such geotextiles and geogrids, resulting from the fact that considerable confinement can be supplied to the compacted infill material by means of the three-dimensional geometry. The strength and the stiffness of geocell-encapsulated soil were studied via triaxial compression tests by Bathurst and Karpurapu (1993) [11], Rajagopal et al. (1999) [12], Chen et al. (2013a) [13], and Song et al. (2019a) [14]. An analytical approach for predicting the stress–strain relationship of the geocell–soil composite was developed by Song et al. (2020, 2022) [15,16] and its effectiveness and reliability were validated via triaxial compression tests of geocell-reinforced soil. Laboratory-scale model tests, centrifuge model tests, limit equilibrium analysis, numerical simulation, and field monitoring were conducted by Chen and Chiu (2008) [17], Xie and Yang (2009) [18], Chen et al. (2013b) [19], and Song et al. (2014, 2017, 2018a, 2018b and 2019b) [20–24] to investigate the deformation characteristic, the failure mechanism of geocell-reinforced retaining walls, and the influencing factors. Geocells were used as a buffer system behind the conventional rigid retaining wall by Kurihashi et al. (2020) [25] to reduce the impact of rockfall, and they discovered that it performed better than sand in this capacity. A thorough analysis of the existing study findings reveals that geocell reinforcement for retaining walls, slopes, and foundations has been employed in engineering and has shown positive reinforcing effects. However, the research on geocell reinforcement of road milling materials is very limited. Geocells have an excellent application potential for reinforcing road milling materials because of their strong reinforcement impact.

In order to explore the mechanical characteristics of geocell-reinforced road milling materials and evaluate the feasibility of using them as the infilled backfill of the geocell-reinforced retaining walls, triaxial compression tests were carried out on the gravels, the surface–base milling mixtures, and the surface milling materials under different confining pressures. On this basis, the analytical model for predicting the stress–strain responses of a geocell–soil composite was adopted for estimating the strength and stiffness of the surface–base milling mixtures and the surface milling materials encapsulated via geocell. For the geocell-encased surface–base milling mixtures, the generalized stress–dilatancy relationship proposed by Pastor et al. (1985) [26] and Duncan et al. (1980) [27] was used to consider the dilatancy, but for the geocell-encased surface milling materials, the tangent Poisson's ratio of the Duncan–Chang model was used to calculate the volumetric contraction. Furthermore, the finite element strength reduction method (SRM) in ABAQUS was adopted to investigate the failure mode and the safety factor of retaining walls made of geocell-reinforced road milling materials. The research results can provide a new idea and reference value for the engineering application of the waste road milling materials.

2. Mechanical Properties of Testing Materials

2.1. Experimental Materials

As shown in Figure 1, the three kinds of test materials were the gravels, the surface asphalt milling materials, and the surface–base milling mixtures in road engineering, which was made by mixing the surface asphalt milling materials and the base milling materials together with a blending ratio of 1:1 (Tian et al., 2020 [28]; Ren et al., 2020 [29]). According to the screening test, the particle sizes of gravel are primarily concentrated in the range of 5–20 mm, while the particle sizes of the surface asphalt milling materials are mainly concentrated in the range of 1–40 mm. The surface–base milling mixtures typically have particle sizes between 0.25 mm and 40 mm. The particle gradation curves of the three test materials are shown in Figure 2. The physical property parameters for the three kinds of materials are listed in Table 1.
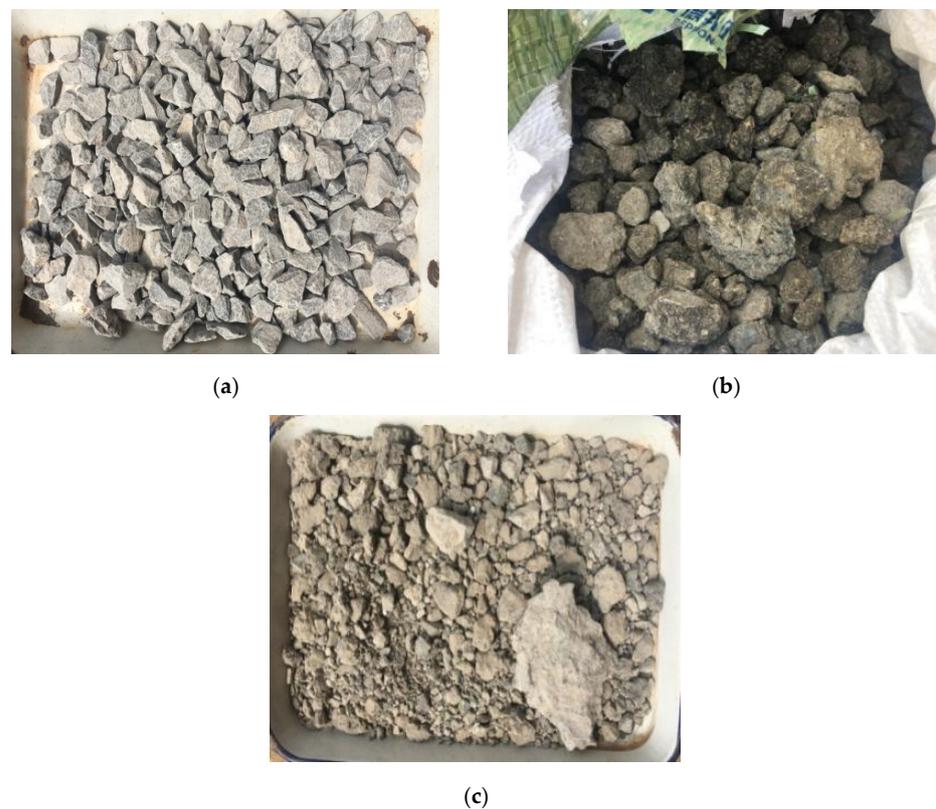

(**a**)

(**b**)

(**c**)

Figure 1. Photos of testing materials. (**a**) Gravels. (**b**) Surface asphalt milling materials. (**c**) Surface–base milling mixtures.
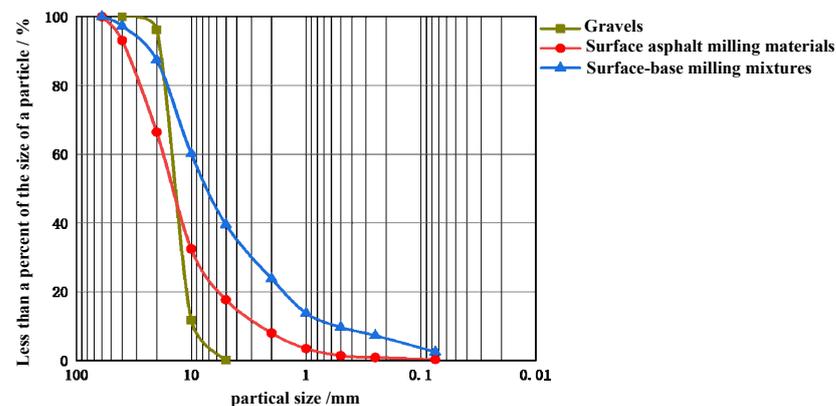

Figure 2. Grading curve of testing materials.

Table 1. Physical properties of testing materials.

Experimental Material	Specific Density of Soil, G_s	d_{60} (mm)	Nonuniform Coefficient, C_u	Coefficient of Curvature, C_c	Maximum Dry Unit Weight, $\gamma_{d,max}$/(kN/m³)	Minimum Dry Unit Weight, $\gamma_{d,mix}$/(kN/m³)
Gravels	2.75	15.5	1.614	1.050	17.39	13.3
Surface–base milling mixtures	2.62	10	19.231	1.731	18.31	13.2
Surface milling materials	2.63	18.3	7.176	1.853	18.57	14.16

2.2. Triaxial Stress–Strain Responses of Infill Materials

Triaxial shear tests were conducted on the three kinds of test materials under the confining pressures of 100 kPa, 200 kPa, 300 kPa, and 400 kPa. On the basis of the analysis of the test results, the relationship between the deviatoric stress and the axial strain and that between the volumetric strain and the axial strain were given and are shown in Figure 3a–c.
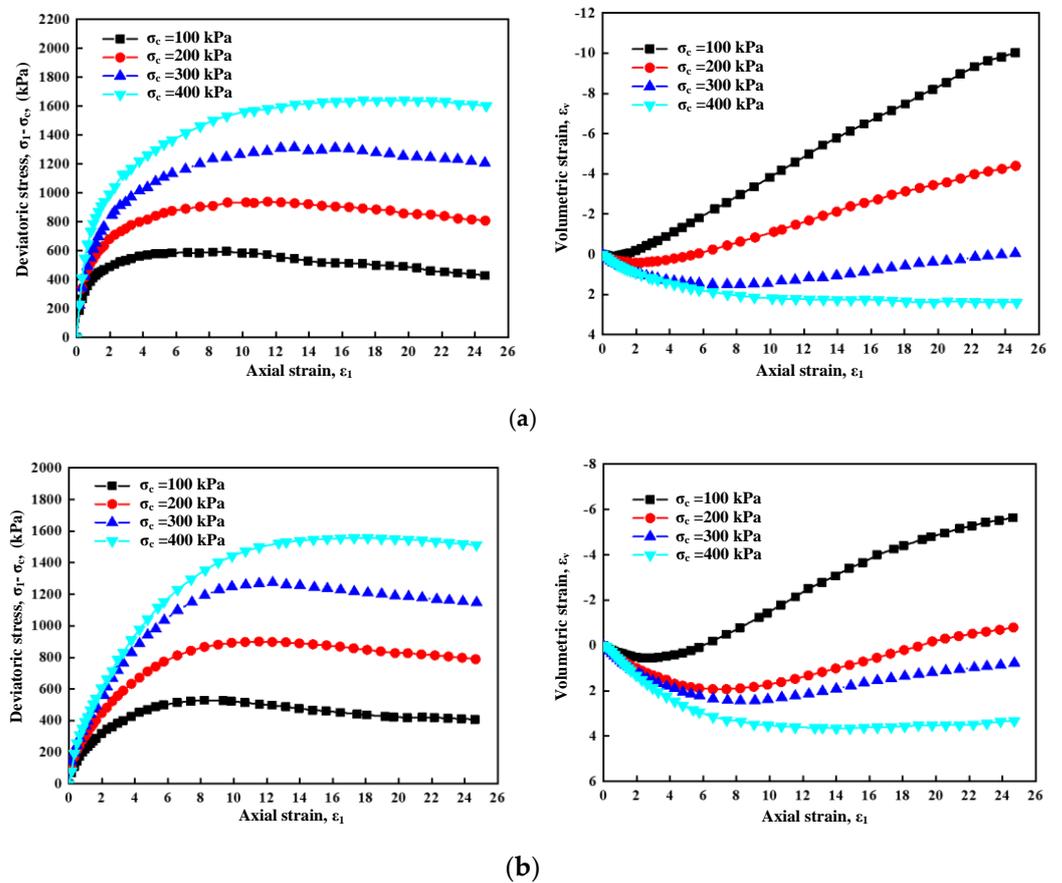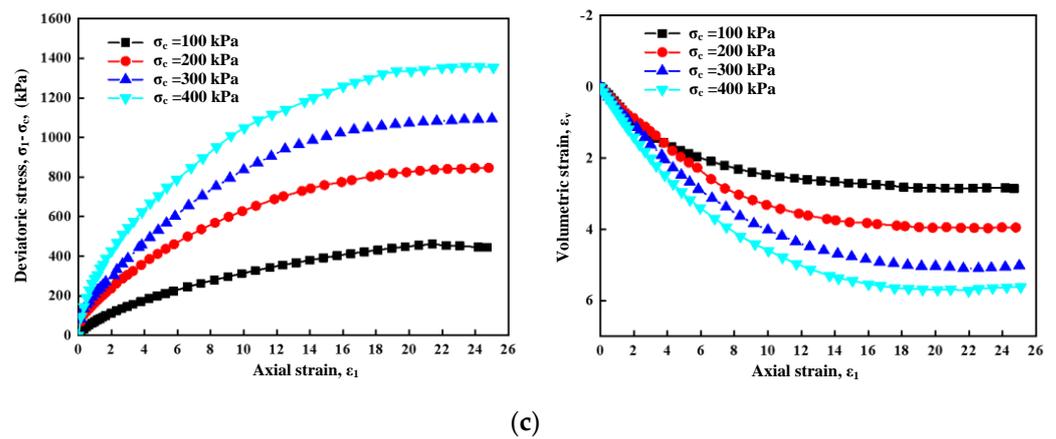

(**a**)

(**b**)

Figure 3. *Cont.*

(c)

Figure 3. Stress–strain relationships of testing materials. (**a**) Gravels. (**b**) Surface–base milling mixtures. (**c**) Surface milling materials.

It can be observed from Figure 3a,b that the stress–strain relationships of the gravels and the surface–base milling mixtures have the similar characteristics. For the two kinds of materials, with the continuous increase in the axial strain, the deviatoric stress also increases gradually, reaches the peak strength, then smoothly decreases to the residual strength, and finally tends to be stable, which indicates that the two test materials exhibit strain-softening characteristics. On the contrary, the deviatoric stress of the surface milling materials increases almost linearly with the increase in the axial strain, and then the deviatoric stress value tends to be stable without an obvious peak value, showing strain-hardening characteristics, which can be observed from Figure 3c. For the gravels and the surface–base milling mixtures, when the confining pressure gradually increases from 100 kPa to 400 kPa, the axial strain to reach the peak deviatoric stress gradually increases, indicating that the characteristics of the test material change from brittleness to ductility. Meanwhile, the peak deviatoric stress of the three test materials all increase with the increase in confining pressures. The peak deviatoric stress of the gravel, the surface–base milling mixtures, and the surface milling materials reached about 1643 kPa, 1557 kPa and 1358 kPa, respectively. Compared with the peak value of the confining pressure of 100 kPa, the increase rate of deviatoric stress was up to 66%, 63%, and 65% under confining pressures of 200 kPa, 300 kPa, and 400 kPa, respectively.

The volumetric strain of the three kinds of materials, as illustrated in Figure 3a–c, can be divided into two stages during the shearing process. At the initial shearing stage (the axial strain smaller than 2%), the three test materials show the characteristics of shear contraction. With the increase in the axial strain, the surface milling materials still show the shear contraction characteristic, but the gravels and the mixture of surface and base milling materials exhibit the dilatancy characteristic. The dilatancy tendency of the gravels is stronger than that of the surface–base milling mixtures, but there is no volumetric dilatancy for the surface milling materials.

2.3. Load–Strain Behavior of Geocell Sheet

Figure 4 shows the tensile stress–strain relationship curve of the high-density polyethylene (HDPE) geocell strip. By fitting the tensile stress–strain test curves of the HDPE geocell strip, the tensile force and the tangent modulus obtained can be expressed as:

$$\frac{T}{T_{ref}} = A_0\varepsilon_1^8 + A_1\varepsilon_1^7 + A_2\varepsilon_1^6 + A_3\varepsilon_1^5 + A_4\varepsilon_1^4 + A_5\varepsilon_1^3 + A_6\varepsilon_1^2 + A_7\varepsilon_1 + A_8 \tag{1}$$

$$\frac{M_t}{M_{ref}} = 8A_0\varepsilon_1^7 + 7A_1\varepsilon_1^6 + 6A_2\varepsilon_1^5 + 5A_3\varepsilon_1^4 + 4A_4\varepsilon_1^3 + 3A_5\varepsilon_1^2 + 2A_6\varepsilon_1 + A_7 \tag{2}$$

where $A_0 \sim A_8$ are the coefficients determined by fitting the tensile test curve, and they are $-152{,}610{,}589{,}250.8$, $70{,}718{,}046{,}117.0$, $-13{,}248{,}194{,}636.9$, $1{,}279{,}287{,}338.6$, $-66{,}812{,}982.1$, $1{,}815{,}037.2$, $-28{,}077.2$, 840.6, and -0.065 for the HDPE sheet in the present study. T_{ref} and M_{ref} are the reference tensile force and modulus, respectively, the values of which are both 1 kN/m.
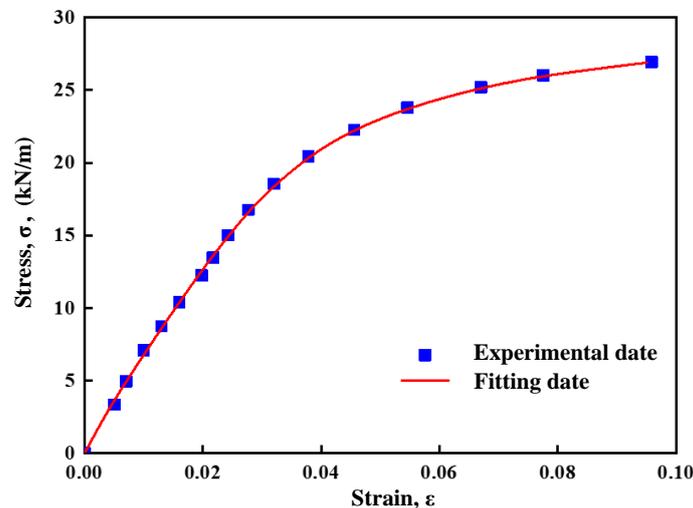

Figure 4. Tensile stress–strain curve of HDPE geocell sheets.

It can be seen from Figure 4 that the fitting results show good agreement with the experimental data, indicating the accuracy of the above coefficients.

3. Stress–Strain Responses of Geocell-Reinforced Road Milling Materials

The surface–base milling mixtures and the road surface milling materials reinforced via geocells were predicted by the analytical method proposed by Song et al. (2020 and 2022) [15,16].

3.1. Analytical Model

For the surface–base milling mixtures, the main stress–strain responses are strain softening and the stress–dilatancy, and the geocell–soil composites composed of such kinds of materials can be predicted via the analytical model proposed by Song et al. (2020 and 2022) [15,16] employing the Mohr–Coulomb yield function and the stress–dilatancy equation in the Pastor–Zienkiewicz (P–Z) model. The method is introduced briefly here.

The relationship between vertical stress increment and horizontal stress increment can be expressed as (Song et al., 2020 and 2022) [15,16]:

$$d\sigma_1 = E_t d\varepsilon_1 + m d\sigma_3 \tag{3}$$

in which $d\sigma_3 = d\sigma_c + d\sigma_g$. σ_c is the small principal stress of the geocell-reinforced soil and σ_g is the additional confining pressure provided by the geocell. E_t is the tangent modulus in the hyperbolic nonlinear model (Duncan et al., 1980) [27], expressed as:

$$E_t = k p_a \left(\frac{\sigma_3}{p_a} \right)^n \left[1 - \frac{R_f (\sigma_1 - \sigma_3)(1 - \sin \varphi)}{2c \cos \varphi + 2\sigma_3 \sin \varphi} \right]^2 \tag{4}$$

in which k = modulus number; n = modulus exponent; R_f = failure ratio; c = soil cohesion; φ = internal friction angle; and p_a = atmospheric pressure.

For sandy soils, the variation of the internal friction angle with the confining pressures can be evaluated by the following equation (Duncan et al., 1980) [27]:

$$\varphi = \varphi_0 - \Delta\varphi lg\left(\frac{\sigma_3}{p_a}\right) \tag{5}$$

where φ_0 is the friction angle at the reference confining pressure and $\Delta\varphi$ is the decrease in friction angle with an increase in the confining pressure.

When selecting the Mohr–Coulomb yield function, the coefficient expressing the relationship between vertical stress increment and horizontal stress increment, m, can be expressed as:

$$m = \frac{1 + \frac{2\eta}{3}}{1 - \frac{\eta}{3}} \tag{6}$$

$$\eta = \frac{q}{p} \tag{7}$$

The incremental form of the additional confining pressure provided by the geocell can be expressed as (Song et al., 2020 and 2022) [15,16]:

$$d\sigma_g = \frac{2M_t}{D_\varepsilon}\frac{d\varepsilon_c}{(1 - \varepsilon_1)} \tag{8}$$

where M_t is the tangent modulus of the cellular geosynthetics. ε_c is the circumferential strain of the geocell when the axial strain reaches ε_1, which can be determined by the following formula:

$$\varepsilon_c = \sqrt{\frac{(1 - \varepsilon_v)}{(1 - \varepsilon_1)}} - 1 \tag{9}$$

D_ε is the equivalent circular diameter of the geocell after deformation when the axial strain reaches ε_1. If D_0 is used to represent the initial equivalent circular diameter of the geocell, the relationship between D_ε and D_0 can be expressed as follows:

$$D_\varepsilon = D_0\sqrt{\frac{(1 - \varepsilon_v)}{(1 - \varepsilon_1)}} \tag{10}$$

where ε_v and ε_1 are the bulk strain and axial strain values of the geocell-reinforced soil complex, respectively.

The volumetric dilatancy of the surface–base milling mixtures can be estimated by the stress–dilatancy equation proposed by Pastor et al. (1985) [26]:

$$\frac{d\varepsilon_v}{d\varepsilon_s} = (1 + \alpha)\left(M - \frac{q}{p}\right) \tag{11}$$

where $d\varepsilon_v$ and $d\varepsilon_s$ are volume strain increment and shear strain increment, respectively.

The stress–strain relationship can be obtained by the iteration and the renewing of stress and strain according to Equations (3)–(11). The iteration proceeds until the stress state of the infill soils satisfies the Mohr–Coulomb criterion or the tensile force in the geosynthetics reaches the geocell joint strength. The detailed iteration process is referred to by Song et al. (2020) [15].

The calculation parameters in the analytical model are all common ones of infill soils and geosynthetics. The nonlinear elastic parameters, the strength parameters, and the parameters describing the volumetric strain of the soils can be determined by three consolidated drained triaxial compression tests under different confining pressures. In addition, the tensile stiffness and the joint strength of the geosynthetics can be determined via the tensile tests.

The research results of Bathurst and Karpurapu (1993) [11], Rajagopal et al. (1999) [12], Chen et al. (2013a) [13], and Song et al. (2019) [14] show that the internal friction angle of geocell-reinforced soil is basically the same as that of unreinforced soil, and the confinement effect of geocells on the infill soil can be regarded as the additional confining pressure. The apparent cohesion caused by this part of confining pressure can be estimated by (Bathurst and Karpurapu, 1993 [11]; Rajagopal et al., 1999 [12]):

$$c_r = \frac{\sigma_g}{2} \tan\left(45° + \frac{\varphi}{2}\right) \tag{12}$$

in which σ_g can be calculated by adding $d\sigma_g$ in each incremental step and φ is the average internal friction angle of the filling in the geocell.

For the pure surface milling materials, the main stress–strain responses are the strain hardening and the volumetric contraction, and the analytical model predicting the geocell–soil composites composed of such kinds of materials is developed here.

According to the generalized Hooke's law, for the infill soils in the geocell, the equation expressing the relationship between the major principal stress increment, the major principal strain increment, and the minor principal stress increment can be written as (Song et al., 2020 and 2022) [15,16]:

$$d\sigma_1 = E_t d\varepsilon_1 + 2v_t d\sigma_3 \tag{13}$$

in which E_t is the tangent modulus expressed as Equation (4) and v_t is tangent Poisson's ratio in the hyperbolic nonlinear model (Duncan et al., 1980) [27] expressed as:

$$v_t = \frac{1}{2} - \frac{E_t}{6B} = \frac{1}{2} - \frac{E_t}{6K_b p_a \left(\frac{\sigma_3}{p_a}\right)^{m_b}} \tag{14}$$

$$B = \frac{(\sigma_1 - \sigma_3)_{70\%}}{3(\varepsilon_v)_{70\%}} \tag{15}$$

where K_b and m_b are the material constants characterizing the volume change, i.e., the intercept and the slope of the straight line representing the relationship between $\lg\left(\frac{B}{P_a}\right)$ and $\lg\left(\frac{\sigma_3}{P_a}\right)$, respectively. $(\sigma_1 - \sigma_3)_{70\%}$ is 70% of the peak deviatoric stress and $(\varepsilon_v)_{70\%}$ is the corresponding volumetric strain at $(\sigma_1 - \sigma_3)_{70\%}$.

The incremental form of σ_g can be written as:

$$d\sigma_g = \frac{2M_t}{D_\varepsilon(1 - \varepsilon_1)} \left[\frac{AE_t v_t d\varepsilon_1}{(1 - v_t - 2v_t^2)} - Ad\sigma_c \right] \tag{16}$$

$$A = \frac{D_\varepsilon(1 - \varepsilon_1)(1 - v_t - 2v_t^2)}{E_t D_\varepsilon(1 - \varepsilon_1) + 2M_t(1 - v_t - 2v_t^2)} \tag{17}$$

Based on the generalized Hooke's law, the volumetric strain for calculating D_ε in Equation (16) was derived and expressed as:

$$d\varepsilon_v = 2Ad\sigma_c + \frac{1 - 2AE_t v_t - v_t - 2v_t^2}{1 - v_t - 2v_t^2} d\varepsilon_1 \tag{18}$$

By substituting Equation (16) into Equation (13), the following equation can be developed for the geocell–soil composite:

$$d\sigma_1 = E_{tc} d\varepsilon_1 + 2v_{tc} d\sigma_c \tag{19}$$

$$E_{tc} = E_t \left[1 + \frac{4v_t^2 M_t A}{D_\varepsilon (1 - \varepsilon_1)(1 - v_t - 2v_t^2)} \right] \tag{20}$$

$$v_{tc} = v_t \left[1 - \frac{2M_t A}{D_\varepsilon (1 - \varepsilon_1)} \right] \tag{21}$$

where E_{tc} and v_{tc} are the tangent modulus and Poisson's ratio of the geocell–soil composite, respectively.

3.2. Stress–Strain Responses

Based on the triaxial compression test results of the surface–base milling mixtures in Figure 3b, the parameters k, n, R_f, φ_0, and $\Delta\varphi$ in the hyperbolic nonlinear model were calibrated as 365.6, 0.148, 0.81, 46.47°, and 8.35°, respectively, and the parameters describing the volumetric strain, φ_{cr} and α, were 40 and 0.4, respectively. For the surface–base milling mixtures reinforced by HDPE geocells with a pocket size of 400 mm × 400 mm, the stress–strain responses under the confining pressures of 50 kPa, 75 kPa, and 100 kPa were predicted via the above analytical model and are illustrated in Figure 5. As can be seen from the figure, for the small axial strain, the deviatoric stress of the reinforced surface–base milling mixtures is smaller than that of the gravels. However, the deviatoric stress of the reinforced surface–base milling mixtures gradually becomes larger than that of the gravels with the increase in the axial strain. For example, when the axial strain is 0.042, the deviation stress of the gravels is 349.4~549.8 kPa and that of the geocell-reinforced surface milling material is 676.1 kPa~701.8 kPa, which is 1.94~1.27 times of that of gravel. It can be seen that the strength of the surface–base milling mixtures reinforced by geocells is obviously higher than that of gravel, while the lateral deformation is smaller than that of gravel, indicating that the reinforcement with geocells can well limit the lateral deformation and improve the strength of surface–base milling mixtures, resulting in the potential to replace the gravels in engineering applications.
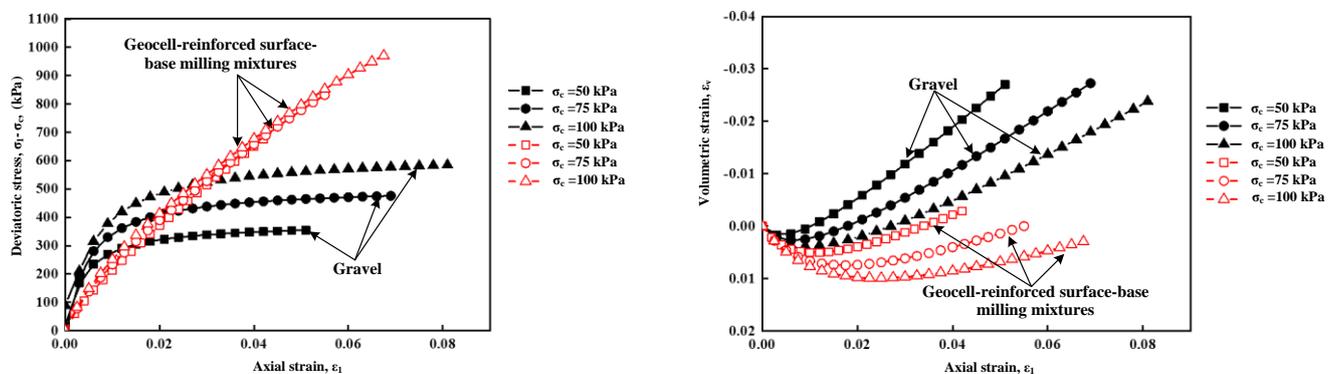

Figure 5. Stress–strain relationships of geocell-reinforced surface–base milling mixtures.

On the basis of the triaxial compression test results of the surface milling materials in Figure 3c, the parameters k, n, R_f, c, and φ in the hyperbolic nonlinear model were calibrated as 60.62, 0.967, 0.682, 43.3, and 37°, respectively, and the parameters describing the volumetric strain, K_b and m_b, were 46 and 0.42, respectively. For the road surface milling materials reinforced via HDPE geocells with a pocket size of 400 mm × 400 mm, the variation of the deviatoric stress and the volumetric strain with the axial strain was predicted via the above analytical model and is shown in Figure 6, from which it can be seen that when the axial strain is small, the difference between the deviatoric stress of the reinforced surface milling materials and that of the gravels is large. However, the difference decreases with an increase in the axial strain. The stiffness and the strength of the reinforced surface milling materials are still smaller than those of the gravels, indicating that they are not suitable to be used in engineering practices. In addition, the volumetric strain of

the gravels is dilatancy, while that of the geocell-reinforced surface milling materials is contraction, indicating that the lateral deformation can be restricted.
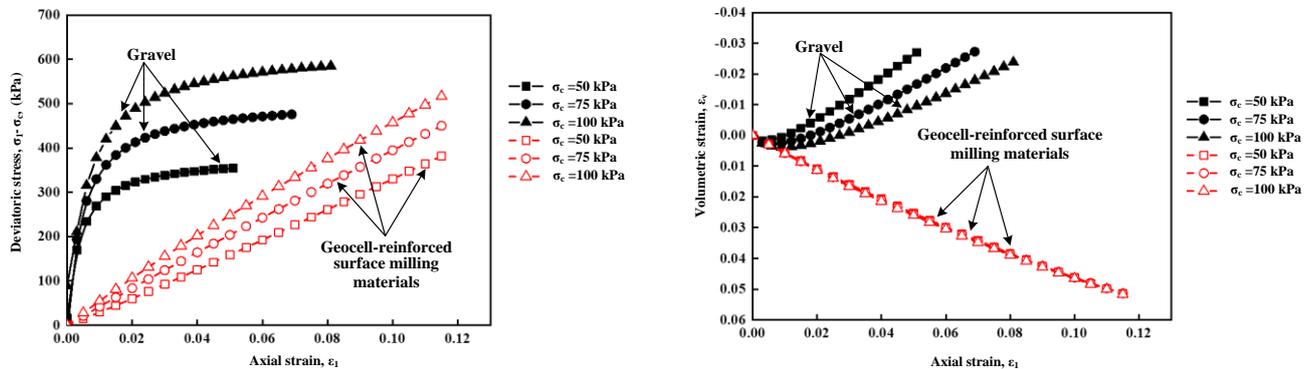

Figure 6. Stress–strain relationships of geocell-reinforced surface milling materials.

4. Parameter Sensitivity Analysis

In order to achieve the optimal reinforcement effect of the geocell, taking the geocell-reinforced surface–base milling mixtures as an example, the effects of main parameters, such as the equivalent circle diameter, D_0, the tangent modulus, M_t, and the peak internal friction angle, φ_o, on the performance of the geocell–soil composite were examined.

4.1. Influence of Geocell Pocket Size

The equivalent circle diameters of the geocells in the analysis were selected as 225.7 mm, 338.5 mm, and 451.4 mm, representing geocell pocket sizes of 200 mm × 200 mm, 300 mm × 300 mm, and 400 mm × 400 mm, respectively. The stress–strain relationship curves of surface–base milling mixtures reinforced by geocells with different D_0-values were analyzed and are illustrated in Figures 7 and 8, respectively.
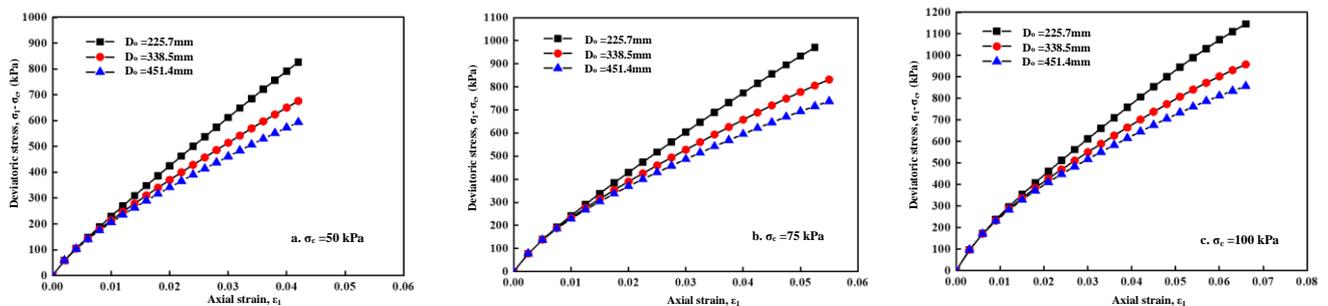

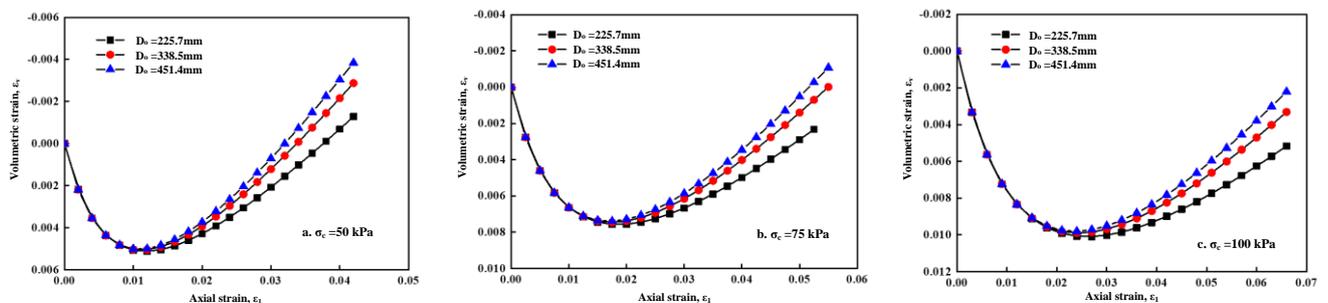**Figure 7.** Variation of deviatoric stress with axial strain for different D_0-values.

Figure 8. Variation of volumetric strain with axial strain for different D_0-values.

It can be observed for Figure 7 that the variation trend of deviation stress–axial strain is basically the same when the confining pressures are 50 kPa, 75 kPa, and 100 kPa, respectively. Therefore, taking the deviatoric stress under the confining pressure of 100 kPa

as an example, when the axial strain is 0.042, the deviatoric stress of $D_0 = 225.7$ mm is 1.15 times that of $D_0 = 338.5$ mm, and the deviatoric stress of $D_0 = 451.4$ mm is 0.92 times that of $D_0 = 338.5$ mm. Thus, when the axial strain is equal, the larger the diameter of the equivalent circle is, the smaller the deviatoric stress reaches. It can be seen that the change of equivalent circle diameter has a great influence on the peak deviation stress, that is, on the strength of reinforced surface–base milling mixtures.

Similarly, the volumetric strain of the geocell-reinforced milling mixtures under the confining pressure of 100 kPa in Figure 8 is taken and analyzed as an example. When the axial strain is 0.042, the equivalent diameter D_0 increases from 225.7 mm to 451.4 mm, and the volume strain changes only by about 5.18%. When the axial strain is equal, the contraction trend of the volumetric strain is strengthened and the dilatancy trend is weakened with a decrease in the equivalent circle diameter, but the change is small. Thus, it can be concluded that the change of equivalent circle diameter has little influence on the volumetric strain.

4.2. Influence of Tangent Modulus

According to the analytical model developed above, the tangent modulus of the geocell is a key parameter affecting the stiffness and the strength of the geocell–soil composite. Therefore, it is of vital importance to explore the effects of the tangent modulus on the strength and deformation characteristics of geocell-reinforced surface–base milling mixtures. An amplification or reduction coefficient, B_m, was defined as:

$$B_m = M_{t_1} / M_t \tag{22}$$

in which M_t is the tangent modulus determined by Equation (2) and M_{t1} is the tangent modulus after amplification or reduction.

The stress–strain responses of geocell-reinforced surface–base milling mixtures under different confining pressures with $B_m = 0.5$, 1.0, and 1.5 were predicted and are illustrated in Figures 9 and 10, respectively. Taking the variation of the deviatoric stress under 100 kPa as an example, it can be seen from Figure 9 that when the axial strain is 0.042, the deviatoric stress is 588.1 kPa~806.6 kPa for $B_m = 0.5$~1.5, and the variation range is 0.84~1.15. When the axial strain is equal, the larger the tangent modulus of the geocell is, the larger the deviatoric stress becomes. It can be seen that the change of the tangent modulus of the geocell has a great influence on the deviatoric stress, i.e., the strength of the geocell-reinforced surface–base milling mixtures in engineering practices.

As can be seen from Figure 10, when the axial strain is 0.042, the volumetric strain changes by 11.96% for $B_m = 0.5$~1.5. Under the condition that the axial strain is equal, the volumetric dilatancy decreases and the contraction strengthens with an increase in the geocell modulus, but the change is not significant. It can be concluded that the change of the modulus of the geocell has small effects on the volumetric strain.
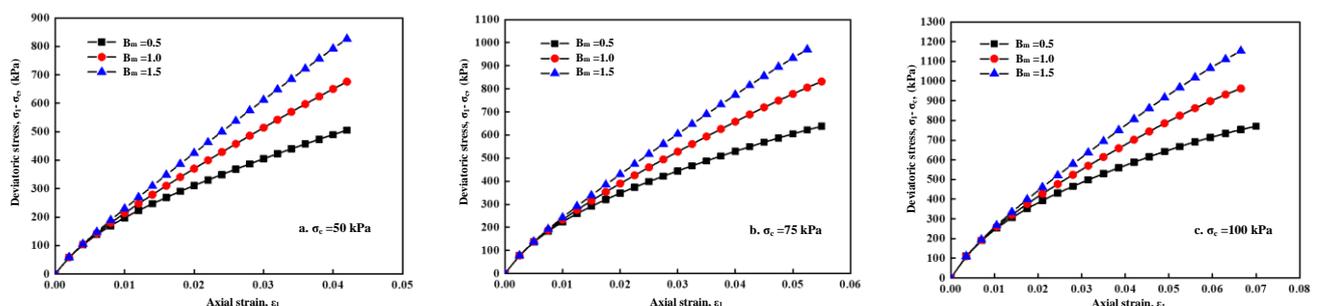

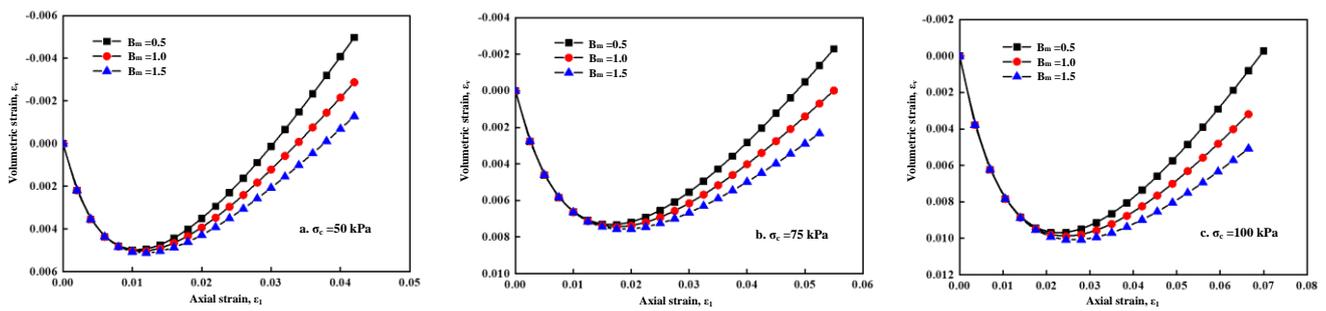**Figure 9.** Variation of deviatoric stress with axial strain for different M_t-values.

Figure 10. Variation of volumetric strain with axial strain for different M_t-values.

4.3. Influence of Peak Internal Friction Angle

According to the above developed analytical model, the peak internal friction angle greatly influences the strength and deformation characteristics of a geocell–soil composite. Therefore, it is necessary to investigate the influence of the peak internal friction angle on the strength and deformation of the geocell-reinforced surface–base milling mixtures.

The stress–strain relationships of the geocell-reinforced milling mixtures under different confining pressures with φ_o = 42°, 44°, and 46° are shown in Figures 11 and 12, respectively. It can be seen from Figure 11 that under the confining pressure of 100 kPa, when the axial strain is 0.042, the deviation stress is within the range of 676.08 kPa to 970.49 kPa for φ_o = 42°, 44°, and 46°. The results show that when the axial strain is equal, the influence of the peak internal friction angle on the deviatoric stress is larger.
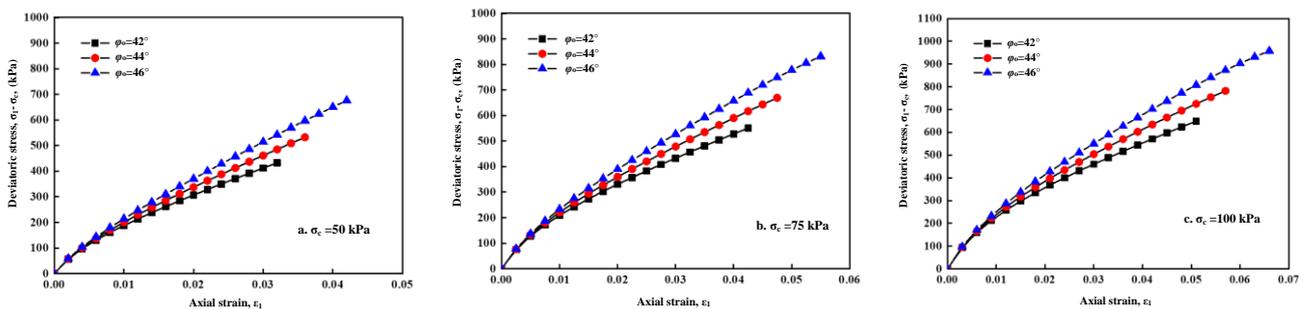

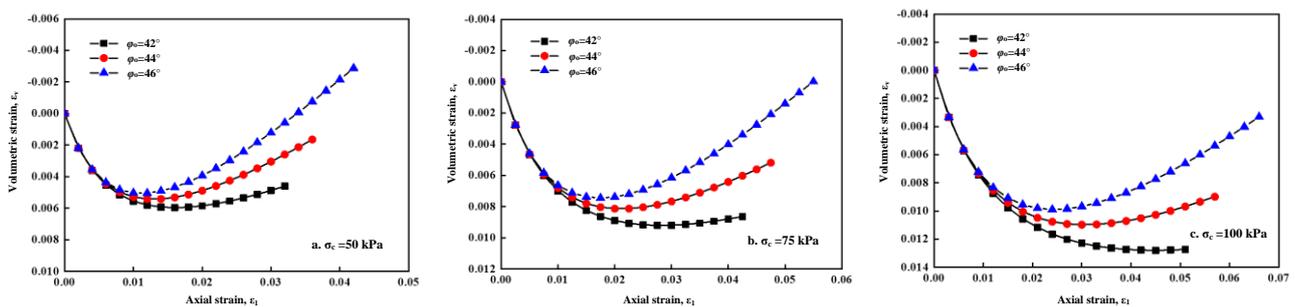**Figure 11.** Variation of deviatoric stress with axial strain for different φ-values.

Figure 12. Variation of volumetric strain with axial strain for different φ-values.

Similarly, it can be observed from Figure 12 that when the axial strain is 0.042, the volumetric strain varies from −0.00216 to 0.0085 for φ_o = 42°, 44°, and 46°, and the variation range is small. When the axial strain is equal, the larger the peak internal friction angle is, the smaller the volumetric strain is. However, the influence of the peak internal friction angle on the volumetric strain of the geocell-reinforced surface–base milling mixtures is not significant.

5. Stability Analysis of Reinforced Retaining Wall

5.1. Analysis Models

It can be concluded from the parametric analysis that the geocell pocket size has a great influence on the strength and deformation of the reinforced surface–base milling mixtures. Here, the finite element strength reduction method in ABAQUS software was employed for the stability analysis of the retaining walls made of geocell-reinforced surface–base milling mixtures. The failure mode and the factor of safety of the retaining walls with the geocell sizes of 200 mm × 200 mm, 300 mm × 300 mm, and 400 mm × 400 mm were investigated. For the comparison, stability analysis of the embankments made of gravels was also conducted.

Figure 13 shows the geometric size of the analyzed model of the geocell-reinforced retaining wall, which was divided into four parts, i.e., the retaining wall body, the backfill, the foundation soil, and the cement–gravel footing, and the material parameters are listed in Table 2. In the simulation, the geocell and the infill soils were treated as composites. The elastoplastic model obeying the Drucker–Prager criterion was used as the constitutive model of the wall body, the backfill, and the foundation soil and the linear elastic model was selected as that of the cement–gravel footing. The internal friction angle of the geocell-reinforced soils was the same as that of the infill, but the apparent cohesion induced by the geocell confinement was estimated via the analytical model in Section 3.1 and is listed in Table 3. In the analysis, the mean confining pressure from the wall top to the bottom, 50 kPa, was used as the confining pressure of the geocell-reinforced soil, σ_c. Tie constraints were set at the interfaces between the backfill base and the foundation soil, between the wall bottom and the footing top, and between the footing and the foundation soil. Surface-to-surface contacts with a friction angle of 27° were set at the interface between the geocell-encased soils and the backfill. The left-side and right-side boundaries of the model were restrained from moving laterally but allowed to move vertically, and the base of the foundation was fixed both in the horizontal and vertical directions. Bilinear plane strain quadrilateral elements (CPE4) were used for the whole model. The whole model was divided into 43,394 nodes and 42,053 elements. Figure 14 shows the mesh division of the two-dimensional reinforced slope.
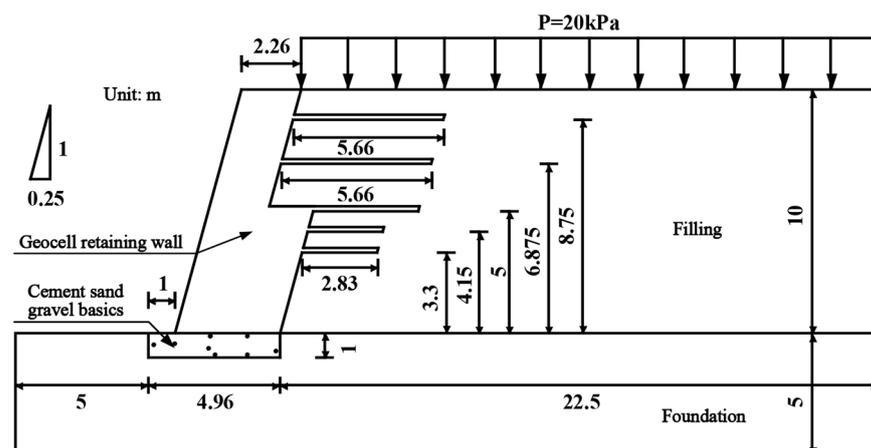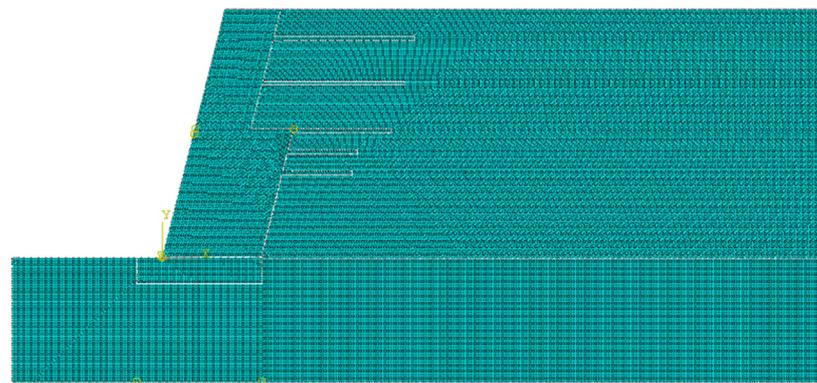

Figure 13. Schematic diagram of the calculation model (unit: m).

Table 2. Mechanical property parameters of the materials.

Experimental Material	Unit Weight γ (kN/m^3)	Elastic Modulus E/MPa	Poisson's Ratio ν	Internal Friction Angle φ/($°$)	Cohesion c/kPa
Geocell-reinforced soil	17.6	90	0.3	43.64	See Table 3
Backfill of gravels	16.7	70	0.35	44.66	0
Backfill of surface–base milling mixtures	17.6	70	0.35	43.64	0
Foundation soil	16.7	300	0.28	34	100
Footing	24	2200	0.17	–	–

Table 3. Apparent cohesion of geocell-reinforced surface–base milling mixtures.

Geocell Pocket Size	Loaded State	Apparent Cohesion, c_r/kPa
200 mm × 200 mm	Ultimate load	150.58
300 mm × 300 mm	Ultimate load	105.77
400 mm × 400 mm	Ultimate load	82.94

Figure 14. Meshing of two-dimensional reinforced slope.

5.2. Analysis of Failure Mode

Figures 15 and 16 show the total displacement contours and the shear strain zone of the gravel embankment and the geocell-reinforced retaining walls, respectively. By reading the coordinates of the total displacement contours in Figure 15, the sliding surfaces of each cases were obtained and are drawn in Figure 17. It can be observed from Figures 15 and 17 that the sliding surface of the gravel embankment is very close to the slope surface and the size of the sliding wedge is relatively small. On the contrary, the sliding surface of retaining walls made of geocell-reinforced surface–base milling mixtures is far away from the slope surface, and the size of the sliding wedge is larger than that of the gravel embankment. In comparison with the gravel embankment, the geocell-reinforced retaining wall shows deep sliding, indicating that the slope stability is strengthened. In addition, the geocell pocket size has a great influence on the slope failure mode. The size of the sliding wedge increases with a decrease in the geocell pocket size. This is because the strength of the geocell-reinforced surface–base milling mixtures increases with a reduction in the geocell pocket size, resulting in a stronger reinforcement effect. It can be seen from Figure 16 that the plastic zone of the gravel embankment penetrates through the slope and forms a continuous sliding zone, but that of the geocell-reinforced retaining walls is not so obvious, indicating that the geocell reinforcement can make the shear strain zone have more diffusion.
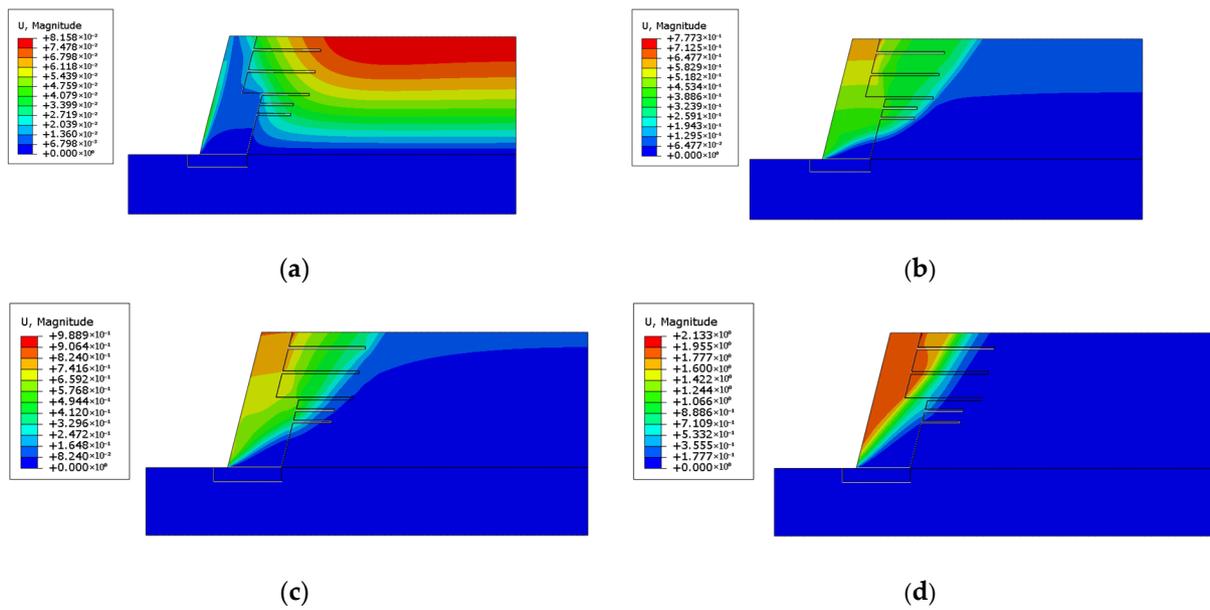
Figure 15. Total displacement contour. (**a**) Gravel embankment. (**b**) Retaining wall reinforced by 200 mm × 200 mm geocell. (**c**) Retaining wall reinforced by 300 mm × 300 mm geocell. (**d**) Retaining wall reinforced by 400 mm × 400 mm geocell.
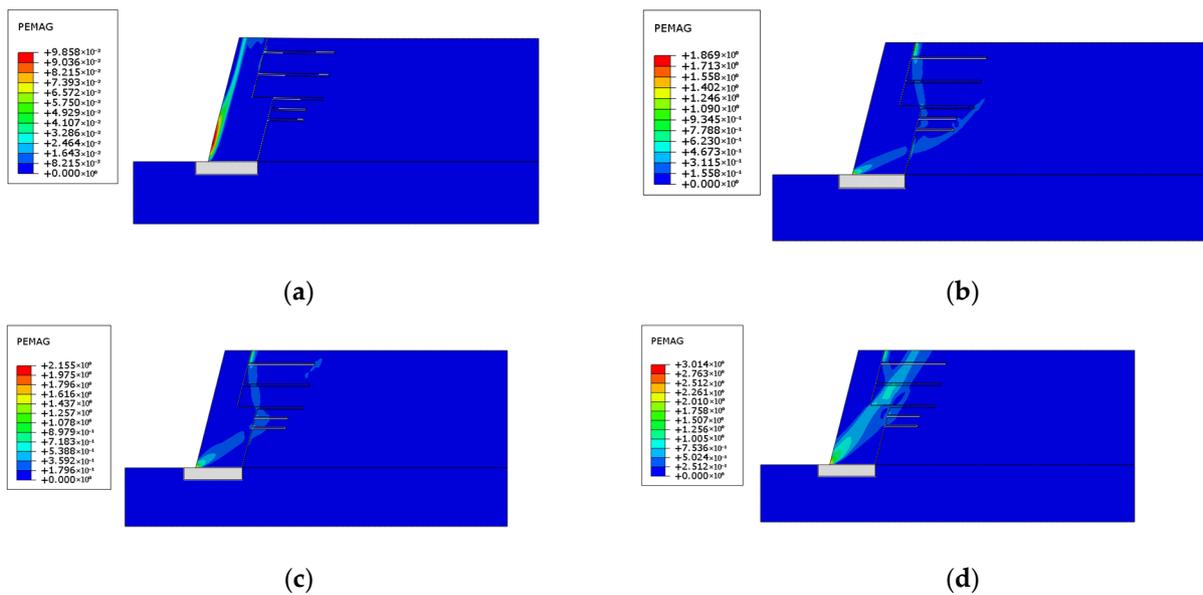

Figure 16. Shear strain zone. (**a**) Gravel embankment. (**b**) Retaining wall reinforced by 200 mm × 200 mm geocell. (**c**) Retaining wall reinforced by 300 mm × 300 mm geocell. (**d**) Retaining wall reinforced by 400 mm × 400 mm geocell.
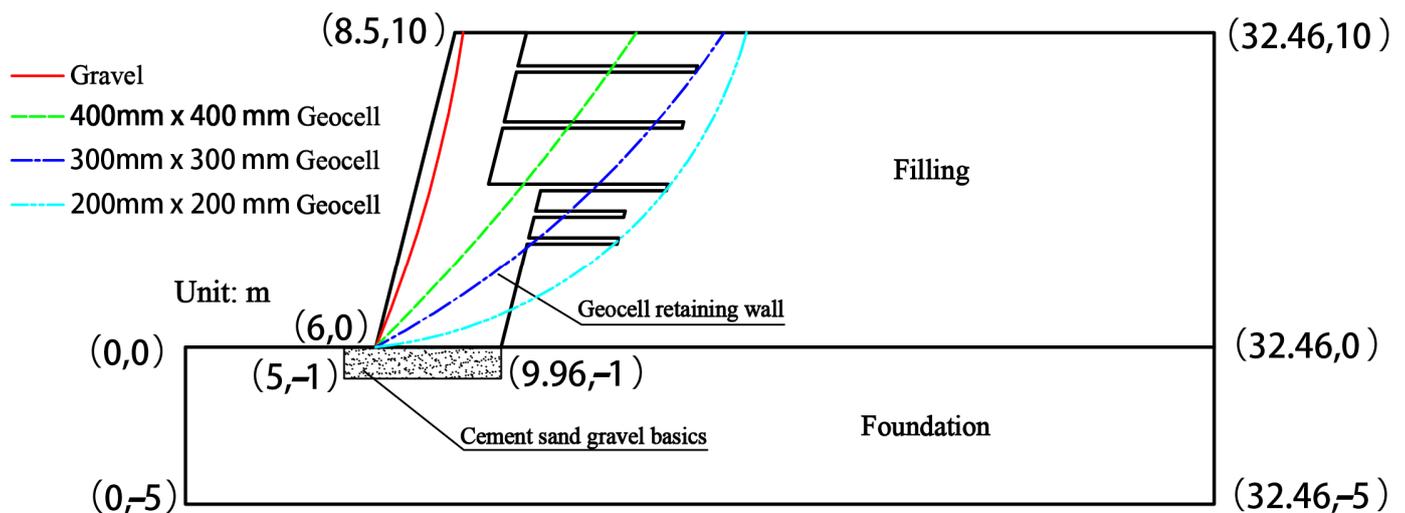
Figure 17. Comparison of sliding faces of each case.

5.3. Analysis of Factor of Safety

The factors of safety (FOS) of the gravel embankment and the geocell-reinforced retaining walls are shown Table 4, from which it can be seen that the FOS of retaining walls made of geocell-reinforced surface–base milling mixtures is much larger than that of the gravel embankment. Compared with the FOS of the gravel embankment, that of the geocell-reinforced retaining wall increases about 4.87~6.35 times, indicating that the stability performance of the retaining wall made of the geocell-reinforced surface–base milling mixtures is greatly improved. The FOS increases with a decrease in the geocell pocket size, resulting from the enhancement of the strength of the geocell–soil composite with a reduction in the pocket size. The FOS of the retaining structures decreases about 29% when the pocket size increases from 200 mm × 200 mm to 400 mm × 400 mm.

Table 4. FOS of gravel embankment and geocell retaining walls.

Retaining Wall Material	Stiffening Condition/(mm^2)	Loaded State	Safety Factor
Gravels	-	Ultimate load	0.381
Geocell-reinforced surface–base milling mixtures	200 mm × 200 mm	Ultimate load	2.419
	300 mm × 300 mm	Ultimate load	2.096
	400 mm × 400 mm	Ultimate load	1.857

It can be seen that, compared with the conventional gravel embankment, the FOS of the retaining walls made of geocell-reinforced surface–base milling mixtures has been significantly improved, and the shallow sliding of the slopes can be significantly prevented. In addition, as a new type of retaining wall structure, the retaining walls made of geocell-reinforced surface–base milling mixtures can reuse the abandoned surface milling materials in road engineering and realize the recycling of engineering waste material, which has important engineering significance. In view of the good engineering performance of the retaining walls made of geocell-reinforced surface–base milling mixtures, and the promotion of the recycling application of waste surface milling material, it will have a wide range of application prospects.

6. Conclusions

(1) The gravels and the surface–base milling mixtures show strain-softening and stress-dilatancy characteristics, while the surface milling materials show strain-hardening and volumetric-contraction characteristics. The strength of the surface milling materials is much lower than that of the gravels and the surface–base milling mixtures.

(2) The strength of the surface milling materials reinforced by geocells is lower than that of the gravels, but the strength of surface–base milling mixtures after geocell reinforcement is higher than that of the gravels. Additionally, the lateral deformation of the surface milling materials and the surface–base milling mixtures with geocell reinforcement is smaller than that of the gravels. Thus, the geocell-reinforced surface–base milling mixtures can be used to replace the gravels in engineering.

(3) The geocell pocket size, the stiffness of the geocell sheet, and the peak internal friction angle all have great influences on the strength of the surface–base milling mixtures reinforced via geocells but little influence on the deformation under different confining pressures. Therefore, the reinforcement effect of geocells can be improved by adjusting the parameter values of D_0, M_t, and φ_0.

(4) The factor of safety of the retaining walls made of geocell-reinforced surface–base milling mixtures is larger than that of the gravels (increases about 4.87~6.35 times), and the smaller the geocell pocket size, the better the stability performance of the retaining wall. In comparison with the gravel embankment, the geocell-reinforced retaining wall shows deep sliding and the size of the sliding wedge enlarges with a reduction in the geocell pocket size. The retaining walls made of geocell-reinforced surface–base milling mixtures can be used to replace gravel embankment in engineering.

References

1. Hessam, S.; Amy, A.K.; Stuart, D.A.; Peter, B. Scenario Planning Application in US Highway Transportation Industry. *J. Infrastruct. Syst.* **2019**, *25*, 05019002.
2. Li, Y.C.; Zhao, L.; Suo, J.J. Comprehensive Assessment on Sustainable Development of Highway Transportation Capacity Based on Entropy Weight and TOPSIS. *Sustainability* **2014**, *6*, 4685–4693. [CrossRef]
3. Li, X.J.; Hu, P.; Li, Y.W.; Liu, S.Q.; Xu, G.X. Study on milling gradation of cold regenerated foamed asphalt mixture. *J. Water Resour. Water Eng.* **2015**, *26*, 200–203.
4. Klauer, K.; Eifler, M.; Kirsch, B.; Seewig, J.; Aurich, J.C. Correlation between different cutting conditions, surface roughness and dimensional accuracy when ball end micro milling material measures with free form surfaces. *Mach. Sci. Technol.* **2020**, *24*, 446–464. [CrossRef]
5. Masi, A.; Bellusci, M.; Carlini, M.; McPhail Stephen, J.; Pumiglia, D.; Reale, P.; Rinaldi, A.; Padella, F. Protective Coating from Manganese Cobalt Oxide Powders Obtained by High Energy Ball Milling: Materials Characterization and Cell Environment Testing. *Meet. Abstr.* **2015**, *3*, 361–363. [CrossRef]
6. Lu, Y.D.; Li, X.J.; Shao, H. Effect of aggregate particle size on regeneration performance of old cement board and water-stable base milling material. *J. Water Resour. Water Eng.* **2015**, *26*, 209–211.
7. Rafiqul, A.T.; Mohiuddin, A.; Mohammad, I.H. Pavement maintenance procedures with and without milling materials. *Int. J. Pavement Res. Technol.* **2016**, *9*, 20–29.
8. Okan, I.; Narayan, S.H.; Dursun, A.K.; Birgul, Z.K. Production of Magnetic Nano-bioconjugates via Ball Milling of Commercial Boron Powder with Biomolecule. *Z. Anorg. Allg. Chem.* **2016**, *642*, 828–832.
9. Wu, J.; Zhang, B.; Wu, C.; Shu, Z.; Li, S.; Yang, J. Discrete element simulation of asphalt pavement milling process to improve the utilization of milled old mixture. *J. Renew. Mater.* **2021**, *9*, 993–1011. [CrossRef]
10. Yu, L.T.; Xie, J.; Li, R.; Hu, J.L.; Pei, J.Z. Study on the performance of emulsified asphalt recycled subgrade based on the evaluation of semi-rigid milling material. *Constr. Build. Mater.* **2022**, *324*, 126614. [CrossRef]

11. Bathurst, R.J.; Karpurapu, R. Large-scale triaxial compression testing of geocell reinforced granular soils. *Geotech. Test. J.* **1993**, *16*, 296–303.

12. Rajagopal, K.; Krishnaswamy, N.R.; Latha, G.M. Behavior of sand confined with single and multiple geocells. *Geotext. Geomembr.* **1999**, *17*, 171–184. [CrossRef]

13. Chen, R.H.; Huang, Y.W.; Huang, F.C. Confinement effect of geocells on sand samples under triaxial compression. *Geotext. Geomembr.* **2013**, *37*, 35–44. [CrossRef]

14. Song, F.; Liu, H.B.; Yang, B.Q.; Zhao, J. Large-scale triaxial compression tests of geocell-reinforced sand. *Geosynth. Int.* **2019**, *26*, 388–395. [CrossRef]

15. Song, F.; Jin, Y.T.; Liu, H.B.; Liu, J. Analyzing the deformation and failure of geosynthetic-encased granular soil in the triaxial stress condition. *Geotext. Geomembr.* **2020**, *48*, 886–896. [CrossRef]

16. Song, F.; Chen, W.S.; Nie, Y.W.; Ma, L.Q. Evaluation of required stiffness and strength of cellular geosynthetics. *Geosynth. Int.* **2022**, *29*, 217–228. [CrossRef]

17. Chen, R.H.; Chiu, Y.M. Model tests of geocell retaining structures. *Geotext. Geomembr.* **2008**, *26*, 56–70. [CrossRef]

18. Xie, Y.L.; Yang, X.H. Characteristics of a new-type geocell flexible retaining wall. *J. Mater. Civ. Eng.* **2009**, *21*, 171–175. [CrossRef]

19. Chen, R.H.; Wu, C.P.; Huang, F.C.; Shen, C.W. Numerical analysis of geocell-reinforced retaining structures. *Geotext. Geomembr.* **2013**, *39*, 51–62. [CrossRef]

20. Song, F.; Xie, Y.L.; Yang, Y.F.; Yang, X.H. Analysis of failure of flexible geocell-reinforced retaining walls in the centrifuge. *Geosynth. Int.* **2014**, *21*, 342–351. [CrossRef]

21. Song, F.; Liu, H.B.; Chai, H.B.; Chen, J.X. Stability analysis of geocell-reinforced retaining walls. *Geosynth. Int.* **2017**, *24*, 442–450. [CrossRef]

22. Song, F.; Liu, H.B.; Hu, H.B.; Xie, Y.L. Centrifuge tests of geocell-reinforced retaining walls at limit equilibrium. *J. Geotech. Geoenviron. Eng. ASCE* **2018**, *144*, 04018005. [CrossRef]

23. Song, F.; Liu, H.B.; Ma, L.Q.; Hu, H.B. Numerical analysis of geocell-reinforced retaining wall failure modes. *Geotext. Geomembr.* **2018**, *46*, 284–296. [CrossRef]

24. Song, F.; Tian, Y.H. Three-dimensional numerical modelling of geocell reinforced soils and its practical application. *Geomech. Eng.* **2019**, *17*, 1–9.

25. Kurihashi, Y.; Oyama, R.; Komuro, M.; Murata, Y.; Watanabe, S. Experimental study on buffering system for concrete retaining walls using geocell filled with single-grain crushed stone. *Int. J. Civ. Eng.* **2020**, *18*, 1097–1111. [CrossRef]

26. Pastor, M.; Zienkiewicz, O.C.; Leung, K.H. Simple model for transient soil loading in earthquake analysis. II: Non-associative models for sands. *Int. J. Numer. Anal. Methods Geomech.* **1985**, *9*, 477–498. [CrossRef]

27. Duncan, J.M.; Byrne, P.; Wong, K.S.; Mabry, P. *Strength, Stress Strain and Bulk Modulus Parameters for Finite Element Analyses of Stresses and Movements in Soil Masses*; Geotechnical Engineering Research Report, No. UCB/GT/80-01; University of California-Berkeley: Berkeley, CA, USA, 1980.

28. Tian, Y.; Niu, D.Y. Milling planer dosage and blending way affect the performance of recycled water stability macadam with. *J. Chang. Univ.* **2020**, *40*, 39–49. (In Chinese)

29. Ren, J.L.; Wang, S.Y.; Zang, G.Y. Effects of recycled aggregate composition on the mechanical characteristics and material design of cement stabilized cold recycling mixtures using road milling materials. *Constr. Build. Mater.* **2020**, *244*, 118329. [CrossRef]